NRCS
Natural Resources Conservation Service
National Soil Survey Center
11 Campus Blvd.
Suite 200
Newtown Square, Pennsylvania 19073

Phone: (610)-557-4233
FAX: (610) 557-4136

Subject: Soils – Geophysical **Date:** 11 October 2012

To: Peter Sussmann
Soil Scientist,
USDA-Forest Service
Region 6, Deschutes National Forest
63095 Deschutes Market Road
Bend, OR 97701

Purpose:
The Ryan Ranch Restoration Project will re-connect the Upper Deschutes River with a historic slough basin floodplain that is approximately 55 acres in size. Concerns have arisen concerning the possible loss of surface water entering the slough basin to deeper aquifers. Ground-penetrating radar (GPR) was used to increase the sampling density, extend information gathered from deep core measurements, and identify stratigraphic variability across the slough basin floodplain.

Principal Participants:
Jim Doolittle, Research Soil Scientist, USDA-NRCS-NSSC, Newtown Square, PA
Jason Gritzner, Hydrologist, USDA-FS, Bend, OR
Peter Sussman, Soil Scientist, USDA-FS, Bend, OR
Bart Wills, Geologist, USDA-FS, Bend, OR
Alex Zglobis, Intern Student Trainee, USDA-FS, Bend, OR

Activities:
All activities were completed on 20-23 August 2012.

Summary:

1. Heterogeneities (e.g., structure and textures) in alluvial sediments affect groundwater flow. Ground-penetrating radar is a powerful tool for delineating heterogeneities in alluvial sediments. Both the 70 and 200 MHz antennas were used to provide insight into the geometry of underlying structures that can influence the flow of ground water within the Ryan Ranch basin meadow.

2. The depth to basaltic rock within the basin meadow was characterized using a 70 MHz antenna. Using a variable propagation velocity model, the average depth to basaltic rock was estimated to be about 7.7 m with a range of 2.3 to 11.8 m. The maximum depth (11.8 m) represents the maximum depth of effective penetration for the 70 MHz antenna in this medium, and therefore, does not represent the maximum depth to basaltic rock within the basin meadow.

3. Spatially, the depth to basaltic rock is greatest in the eastern arm and the central portion of the basin meadow. The western arm of the basin meadow is shallower to basaltic rock.

4. The large-scale stratigraphic architecture across the basin meadow was documented on radar records collected with a 200 MHz antenna and characterized using a facies-based approach. Facies analysis represents a pattern-based approach to interpretation. Six architectural units or

radar facies were identified. It is assumed that the internal structure of the revealed architectural units is relevant to the movement of ground water.

5. The survey area is relatively expansive with both vertical and lateral variability in water and clay contents. This variability affects the dielectric permittivity of the sediments and the propagation velocity used to calculate depths to interfaces on radar records. At the time of the radar survey, no cores were extracted and no time/depth conversions were completed. This was unfortunate, as during the subsequent analysis of the radar records, doubts occurred concerning some depth interpretations. As a consequence, different velocity models have been used to estimate the depths to basaltic rock (used a variable velocity model) and to portray the radar data in three-dimensional simulations (used a constant velocity model).

It was my pleasure to work with you and hopefully to have been of some assistance to you.

Jim Doolittle
Research Soil Scientist
National Soil Survey Center

cc:
Thor Thorson, Acting State Soil Scientist/MLRA Office Leader, USDA-NRCS, 1201 NE Lloyd Blvd., Suite 900, Portland, OR 97232
Larry West, National Leader, Soil Survey Research & Laboratory, USDA-NRCS, MS 41, USDA-NRCS, Lincoln, NE

Background:
The Ryan Ranch restoration project will re-connect the Upper Deschutes River with a historic slough basin on its floodplain. The present basin meadow is below the elevation of natural stream flows in the Upper Deschutes River. This project will restore approximately 55 acres of freshwater emergent wetland habitat by removal of a levee, which has prevented surface water from inundating the basin meadow. The levee was constructed to enhance the delivery of stored irrigation water to downstream users. Concerns regarding the possible loss of surface water entering the basin meadow to deeper aquifers have prompted a detailed study of the regolith in the basin meadow. Cores from twelve deep boreholes, which were drilled into or near the underlying basaltic rock, have revealed complex stratigraphic columns within the basin. The Forest Service requested ground-penetrating radar field assistance to correlate radar signatures with known stratigraphy observed in the boreholes and to expand the knowledge of the stratigraphy and depth to basaltic rock across the basin.

Soils and Sediments:
Soils within the basin meadow range from somewhat poorly drained to very poorly drained and contain strata of alluvial and volcanic sediments. Sediment depths within the meadow were measured with a Geoprobe in October, 2009. Borings revealed Mazama ash tephra layer, layers of mixed alluvium, and highly weathered residuum underlying silty diatomaceous materials. These stratigraphic layers are underlain by highly weathered basaltic rock. Borings did not reveal the depths to unweathered basaltic rock as refusal was encountered in the weathered residuum.

Ground-Penetrating Radar (GPR):
Knowledge of the architecture of fluvial sequences is vital to wetland restoration projects. The architecture of stratigraphic layers in alluvial basins is typically complex, and its reconstruction is difficult and often based on oversimplified assumptions drawn from limited core data. In the absences of continuous and satisfactory outcrops or exposures, GPR is an accepted tool for imaging the regolith (Dagallier et al., 2000; Beres and Haeni, 1991). Ground-penetrating radar can provide information on the underlying soil, stratigraphic column, and bedrock. Ground-penetrating radar has been used extensively to provide high resolution records of alluvial deposits on floodplains (Sambrook Smith et al., 2006; Skelly et al., 2003; Vandenberghe and van Overmeeren, 1999; Bridge et al., 1998; Leclerc and Hickin, 1997; Bridge et al., 1986;) and wetlands (Rubin et al., 2012; Gómez-Ortiz et al., 2010; O'Driscoll et al., 2010). In these studies, GPR was useful for delineating lithofacies and the geometry and orientation of strata associated with channel migration and deposition. In a related study, Rubin et al. (2012) used GPR to map sediments and categorize depositional regimes in a wetland restoration project. In addition, GPR has been widely used to chart bedrock depths (Gerber et al., 2010; Sass 2007; Collins et al., 1989; Davis and Annan, 1989), and fractures, joint patterns, and faults in rock masses (Mysaiah et al., 2011; Theune et al., 2006; Porsani et al., 2005; Nascimento da Silva et al., 2004; Demanet et al., 2001; Lane et al., 2000; Pipan et al., 2000).

Equipment:
The radar unit is the TerraSIRch Subsurface Interface Radar (SIR) System-3000 (here after referred to as the SIR-3000), manufactured by Geophysical Survey Systems, Inc. (GSSI; Salem, NH).[1] The SIR-3000 consists of a digital control unit (DC-3000) with keypad, SVGA video screen, and connector panel. A 10.8-volt lithium-ion rechargeable battery powers the system. The SIR-3000 weighs about 4.1 kg (9 lbs) and is backpack portable. With an antenna, the SIR-3000 requires two people to operate. Jol (2009) and Daniels (2004) discuss the use and operation of GPR. Antennas with center frequencies of 70 and 200 MHz were used in this investigation. The scanning rate of the GPR was set at 20 scan/sec for the 70 MHz antenna and 42 scan/sec for the 200 MHz antenna.

[1] Manufacturer's names are provided for specific information; use does not constitute endorsement.

The RADAN for Windows (version 6.6) software program (developed by GSSI) was used to process the radar records.[1] Processing included: header editing, setting the initial pulse to time zero, color table and transformation selection, signal stacking, horizontal high pass filtration, migration, and range gain adjustments (refer to Jol (2009) and Daniels (2004) for discussions of these techniques). The *Interactive 3D Module* of RADAN was used to semi-automatically "*pick*" the depths to interfaces on radar records. The *picked* data were exported to a worksheet (in an X, Y, and Z format; including longitude, latitude, and depth or two-way travel time to an interface (e.g., basaltic rock surface)).

The SIR-3000 system contains a setup for the use of a GPS receiver with a serial data recorder (SDR). With this setup, each scan of the radar can be georeferenced (position/time matched). Following data collection, a subprogram within the RADAN for Windows was used to proportionally adjust the position of each radar scan according to the time stamp of the two nearest positions recorded with the GPS receiver. A Trimble AgGPS114 L-band DGPS (differential GPS) antenna (Trimble, Sunnyvale, CA) was used to collect position data. [1] Position data were recorded at a rate of one reading per second.

Calibration of GPR:

Ground-penetrating radar is a time scaled system. The system measures the time that it takes electromagnetic energy to travel from an antenna to an interface (e.g., soil horizon, stratigraphic layer, lithologic surface) and back. To convert the travel time into a depth scale, either the velocity of pulse propagation or the depth to a reflector must be known. The relationships among depth (D), two-way pulse travel time (T), and velocity of propagation (v) are described in equation [1] (after Daniels, 2004):

$$v = 2D/T \qquad [1]$$

The velocity of propagation is principally affected by the relative dielectric permittivity (E_r) of the profiled material(s) according to equation [2] (after Daniels, 2004):

$$E_r = (C/v)^2 \qquad [2]$$

Where C is the velocity of light in a vacuum (0.3 m/ns). Typically, velocity is expressed in meters per nanosecond (ns). In soils, the amount and physical state (temperature dependent) of water have the greatest effect on E_r and v. The dielectric permittivity ranges from 1 for air, to 78 to 88 for water (Cassidy, 2009). Small increments in soil moisture can result in a substantial increase in the relative permittivity of soils (Daniels, 2004). Using a 100 MHz antenna, Daniels (2004) observed that the relative dielectric permittivity of most dry mineral soil materials is between 2 and 10, while for most wet mineral soil materials, it is between 10 and 30.

The most accurate method to determine the velocity of propagation is to identify reflectors on GPR records that occur at known depths (Conyers and Goodman, 1997). The two-way pulse travel time to known reflectors can be directly obtained from the radar record. Using the known depth and travel time to a reflector, and equations [1] and [2], the v and E_r can be respectively determined, and the vertical scale on radar records can be converted from a time-scale into a depth-scale.

At the time of the radar survey, no cores were extracted and no time/depth conversions were completed. This was unfortunate. In addition, although nearly level, the survey is large with noticeable differences in soil moisture observed between the drier eastern and wetter western portions of the basin meadow. A large, 2.1 m (7 feet) depression in the eastern portion of the site was dry, but a smaller, 0.61 m (2 feet) depression in the western portion of the site contained standing water. Spatial and vertical variations in soil moisture across the basin meadow will affect the accuracy of all time/depth conversions of radar data.

Radar traverses that were collected with the 70 MHz antenna passed in the vicinity of two wells where the depth to basaltic rock is known. For the data collected with the 70 MHz antenna, the measured depths to basaltic rock at these two wells (# 52 and 53) were used to convert the radar's vertical time-scale into a depth-scale. Based on the measured depths and the two-way pulse travel times to the interpreted basaltic rock surface, the average v and E_r through the overlying column were estimated using equations [1] and [2]. At well # 53, the depth to basaltic rock is 6.85 meters. Based on this depth and the two-way travel time to this interface on the radar record, the estimated average E_r and v were 4.31 and 0.1445 m/ns, respectively. These values imply rather dry earthen materials. This velocity (0.1445 m/ns) was used to depth scale the radar data shown in Figures 3, 5 and 6 of this report (these simulations require a constant velocity of propagation).

At well # 52, the depth to basaltic rock is 10.66 meters. Based on this depth and the two-way travel time to this interface on the radar record, the estimated E_r and v were 12.69 and 0.0842 m/ns, respectively. These values are associated with relatively moist earthen materials. The decrease in velocity at well # 52 is attributed to higher moisture contents at lower depths. The decrease in velocity also reflects the relatively wetter conditions in the western arm of the basin meadow. Based on the measurements from the two wells, for the 70 MHz antenna, the velocity of propagation was proportional adjusted (based on increasing travel time) using the following equation:

$$v = 0.1869 + (-0.00037*T) \qquad [3]$$

Where T is the two-way pulse travel time to the basaltic rock surface. Equations [3] and [1] were used to convert the radar data collected with the 70 MHz antenna from time scale into depth scale measurements. This model was used to construct the two-dimensional (2D) simulation shown in Figures 4 and 8 of this report.

The 200 MHz antenna was used to provide higher resolution, but shallower depth of exploration information. During the course of the survey with the 200 MHz antenna, the GPR passed in the vicinity of thirty-four wells that are scattered across the basin meadow. At most of these wells, the depth to Mazama ash (ranging from 0.66 to 9.96 m) was known. The Mazama ash layer is a major, contrasting stratigraphic contact and generally associated with a high amplitude radar reflection. However, the Mazama ash layer was difficult to consistently identify on radar records. Like other strata appearing on radar records, its reflections varied in amplitude, and were discontinuous and highly variable in depth. As noted by Bayer et al. (2011), in stratified sediments, the identification of a single stratum on radar records is most challenging. As a consequence, the identification of the Mazama ash on radar records proved impractical and its use for time/depth conversions was abandoned.

For data collected with the 200 MHz antenna, "hyperbolic velocity analysis" (see Jol (2009) for discussion of this technique) was used to estimate an average velocity of pulse propagation. In hyperbolic velocity analysis, a velocity is determined by matching the ideal form of a velocity-specific hyperbola function to the observed form of reflection hyperbola appearing on radar records. However, as noted by Cassidy (2009), hyperbolic matching will only produce approximate velocity estimates with errors often greater than 10%. Rather than calculating velocity values for different depth intervals, Cassidy (2009) recommends the use of a constant, average velocity, which produces the "same interpretational results". Following hyperbolic velocity analysis of 89 hyperbolas appearing on 27 radar records, a relatively high correlation ($R^2 = 0.7716$) was observed between the velocity of propagation and the two-way travel time (see Figure 1). As evident in Figure 1, the velocity of propagation decreases with increasing travel time and depth. Based on hyperbolic matching, an average velocity of 0.1547 m/ns and the average dielectric permittivity of 3.76 were used to convert the time-scaled, 200 MHz radar data into a depth-scale measurements that are shown in the three dimensional (3D) simulations of this report (Figures 9 to 14).

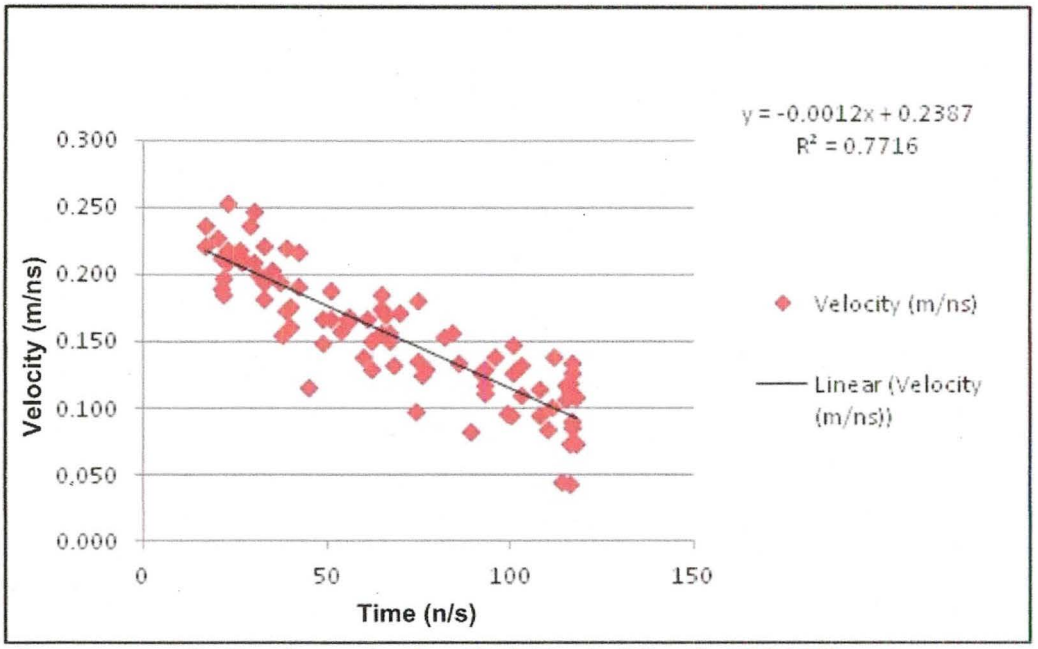

Figure 1. An average velocity of propagation (0.1547 m/ns) for the 200 MHz antenna was estimated using hyperbolic velocity analysis.

Resolution:
Resolution is the ability to resolve targets that are close together as separate features. Resolution is defined as the smallest separation that can be discerned between discrete targets. Ground-penetrating radar provides the highest lateral and vertical resolution of all geophysical method used to image the subsurface. Resolution is largely controlled by the wavelength of the propagating electromagnetic energy and the dielectric permittivity of the profiled materials.

Vertical resolution is dependent on the wavelength (λ). In general, vertical resolution is considered to be about ¼ of the wavelength. In general theory, if two features are separated in time by less than this amount, they will interfere in a constructive manner, resulting in a signal reflection which will be interpreted as a signal event (Neil, 2004). Vertical resolution is controlled by the returned wavelength, which is determined by dividing the propagation velocity (v) by the antenna frequency (f) (after Daniels, 2004):

$$\lambda = \frac{v}{f} \qquad [4]$$

In equation [4], the wavelength is expressed in meters, the velocity in meters/ns, and the frequency in cycles/ns. Vertical resolution increases with increasing frequency (shorter wavelengths) and dielectric permittivity. For the 70 MHz antenna, using an average v of 0.1445 m/ns, the wavelength is 206 cm and the vertical resolution is about 52 cm. For the 200 MHz antenna, using an average v of 0.1547 m/ns, the wavelength is 77 cm and the vertical resolution is about 19 cm. Due to the larger wavelength of the 70 MHz antenna, fewer interfaces can be resolved on radar records.

Study Site:
The site is located in a meadowland along the Upper Deschutes River southwest of Bend. Figure 2 is an image of the study site taken from the Web Soil Survey. Soils within the study site have not been mapped

or digitized. In Figure 2, the basin meadow is clearly evident with variations in tonal patterns associated with differences in meadow vegetation and soil moisture.

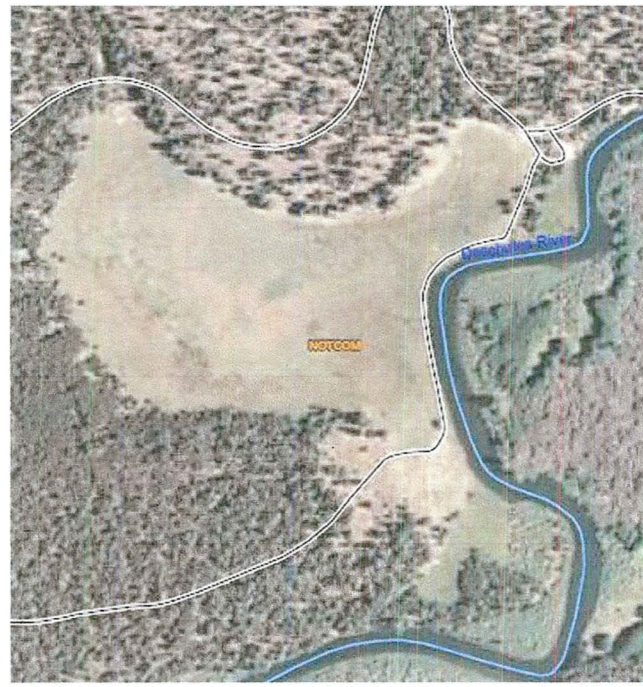

Figure 2. This aerial view shows the meadowland surveyed with GPR as part of the Ryan Ranch Restoration Project.

Survey Procedures:

Multiple, pedestrian surveys were completed with each antenna across the basin meadow. Forty traverses were completed with the 70 MHz antenna. For each of these traverses, the 70 MHz antenna was carried about 12 inches above the ground surface with its long axis parallel to the direction of travel. Because of satellite shading, which prevented the georeferencing of some radar data, and recording problems, only 34 of these traverses were available for interpretation, analysis and plotting. Twenty-seven traverses were completed with the 200 MHz antenna across the basin meadow. For each of these traverses, the 200 MHz antenna was towed along the ground surface. All radar traverses were stored as separate files. For both antennas, the radar traverses that were conducted along the levee suffered from excessive signal attenuation, which seriously reduced exploration depths and the interpretability of subsurface reflections. These traverses were not analyzed or plotted.

Results:

Depth to Basaltic rock:

Figure 3 is a *Google Earth* image of the Ryan Ranch Restoration Site showing the locations of the traverse lines that were completed with the 70 MHz antenna. Colors have been used to identify seven depth-to-basaltic rock groupings. As shown in Figure 3, the seven groups are based on 3.0 m depth intervals. These estimated depths were derived using a constant propagation velocity (v = 0.1445 m/ns), the two-way pulse travel time to the basaltic rock interface (where evident), and equation [1]. Using a constant propagation velocity, the average depth to basaltic rock is about 8.28 m with a range of 1.9 to 18.0 m. Using this model, below a depth of 18.0 m, excessive signal attenuation restricted signal penetration and the basaltic rock interface was not evident on radar records. As a consequence, using a constant velocity of 0.1445 m/ns, the estimated maximum depth (18.0 m) is the deepest effective depth of penetration for the 70 MHz antenna in this medium, and is not representative of the maximum depth to

basaltic rock. It is believed, however, that this constant velocity model has over-estimated the depth to basaltic rock especially where it is the deepest.

In Figure 3, a large area with a depth to basaltic rock > 18 m (colored purple) is evident in the northeastern and central portion of the basin meadow. Here, the depth to basaltic rock is projected (using a constant velocity model) to be greater than 18.0 m, and because of extreme signal attenuation, reflections from the basaltic rock were not visible on radar records.

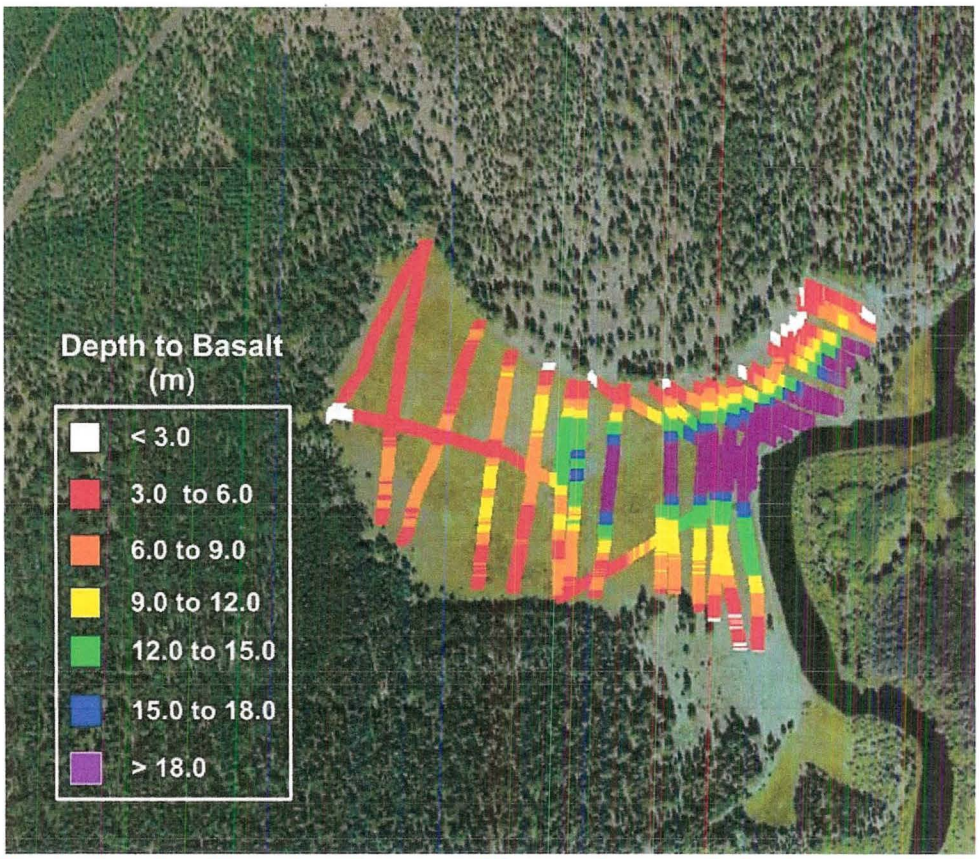

Figure 3. The depth to basaltic rock, as interpreted from radar records, is shown on this Google Earth image (courtesy of Brian Jones of GSSI). All depths are expressed in meters. Depths have been estimated using a constant velocity (0.1445 m/ns)

As evident in Figure 3, the depth to basaltic rock is greatest in the eastern arm and the central portion of the basin meadow. In the immediate area of this large trough or depression in the basaltic rock surface, depth classes appear to change rapidly over short distances, suggesting not only greater relief, but a steeper subsurface topography. The western arm of the basin meadow is shallower to basaltic rock. Here, the changes in the depth to basaltic rock are more gradual and the general subsurface topography of the basaltic rock surface nearly level to gently sloping.

The depths shown in Figure 3 were derived using a constant velocity of propagation. These estimated depths do not account for the decrease in the propagation velocity caused by increasing moisture contents with increasing depth. As a consequence, it must be repeated that the depths shown in Figure 3 are believed to be greater than actual.

Figure 4 is a two-dimensional simulation of the Ryan Ranch Restoration Site showing the interpreted depth to basaltic rock using a variable velocity model. The data for this simulation were derived using

equation [3], which attempts to account for the projected reduction in propagation velocity that is caused by the assumed increase in water content with increasing depth. However, the reduction in v with depth is undoubtedly not constant, as it is influenced by the presence and depth to different strata with contrasting E_r within the profiled materials. In addition, moisture contents are known to be spatially variable across the basin meadow, with the western arm being generally wetter than the eastern arm.

In Figure 4, colors have been used to identify the interpreted depth to bedrock in one meter depth intervals. Estimated depths are based on a variable propagation velocity (estimated using equation [3]), the two-way pulse travel time to the basaltic rock interface, and equation [1]. Using a variable propagation velocity, in these sediments, the average depth to bedrock was estimated to be about 7.7 m with a range of 2.3 to 11.8 m. The maximum depth (11.8 m) represents the maximum depth of effective penetration for the 70 MHz antenna in this medium. Using the variable velocity model, below a depth of 11.8 m, signal attenuation is severe and the identification of the basaltic rock interface is not possible. As evident in Figure 4, a large area in the central and eastern arms of the basin meadow has basaltic rock at depths greater than 11.0 m. Two faint lineations having relatively deeper depths to basaltic rock extend across and towards the northwestern and southwestern corners of the western arm of the basin meadow. These patterns suggest irregular deposition of the basaltic rock and/or erosion caused by former stream channels.

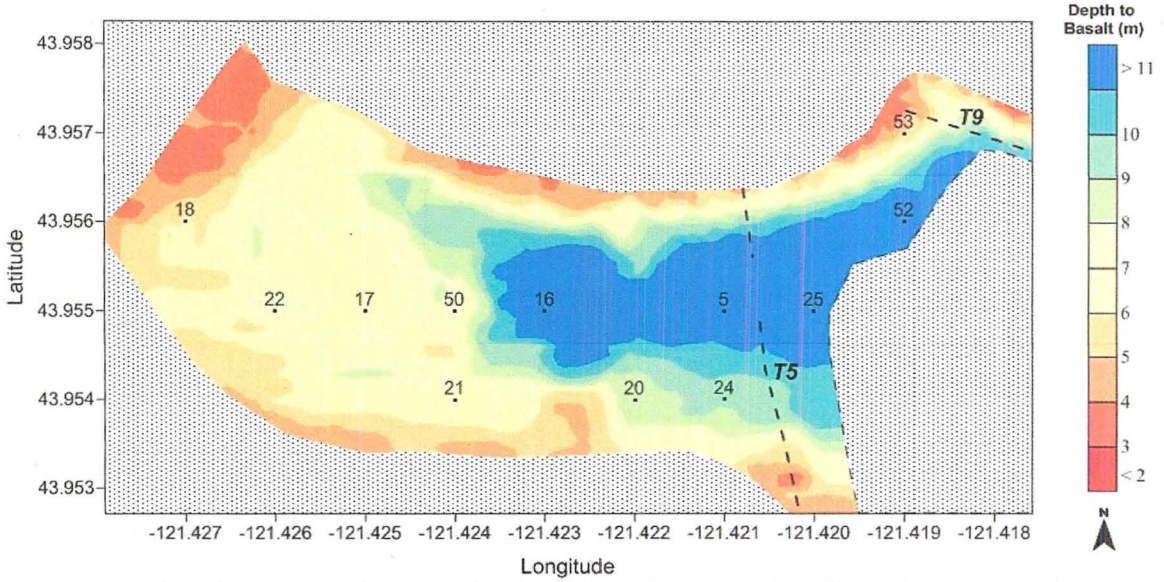

Figure 4. Depth to basaltic rock within the Ryan Ranch Restoration Site as interpreted from radar records using a variable velocity model. Bold numbers identify selected 70 MHz antenna traverse lines (dashed lines) and plain numbers identify well sites. All depths are expressed in meters.

Figures 5 and 6 are three-dimensional (3D) simulations of representative radar records obtained with the 70 MHz antenna from different parts of the basin meadow (see Figure 4 for locations). In each 3D simulation, all measurements are expressed in meters. In these figures, the Universal Transverse Mercator (UTM) geographic coordinate system has been used to georeference the radar traverses. In each 3D simulation, a green-colored, segmented line has been used to approximate the interpreted basaltic rock surface.

Figures 5 is the radar record from traverse line T9 (see Figure 4 for location). This traverse line passed near well # 53, which is located at the bottom of a large, 2.1 m deep depression (near "A" in Figure 4). At the time of this survey, the bottom of this depression was dry.

In Figure 5, the underlying basaltic rock surface provides high-amplitude (colored white and gray) reflections that are easily traced laterally across the radar record. The high reflection amplitudes of this bounding surface suggest strongly contrasting materials on either side of the interface. In the southern (right-hand) part of this radar traverse the basaltic rock surface plunges to greater depths, and as a consequence suffers greater levels of signal attenuation and is more difficult to identify (near "C" in Figure 5). Internal reflections from the basaltic rock suggest the presence of different layers, each characterized by contrasting spatial reflection patterns (frequency, amplitude, geometry).

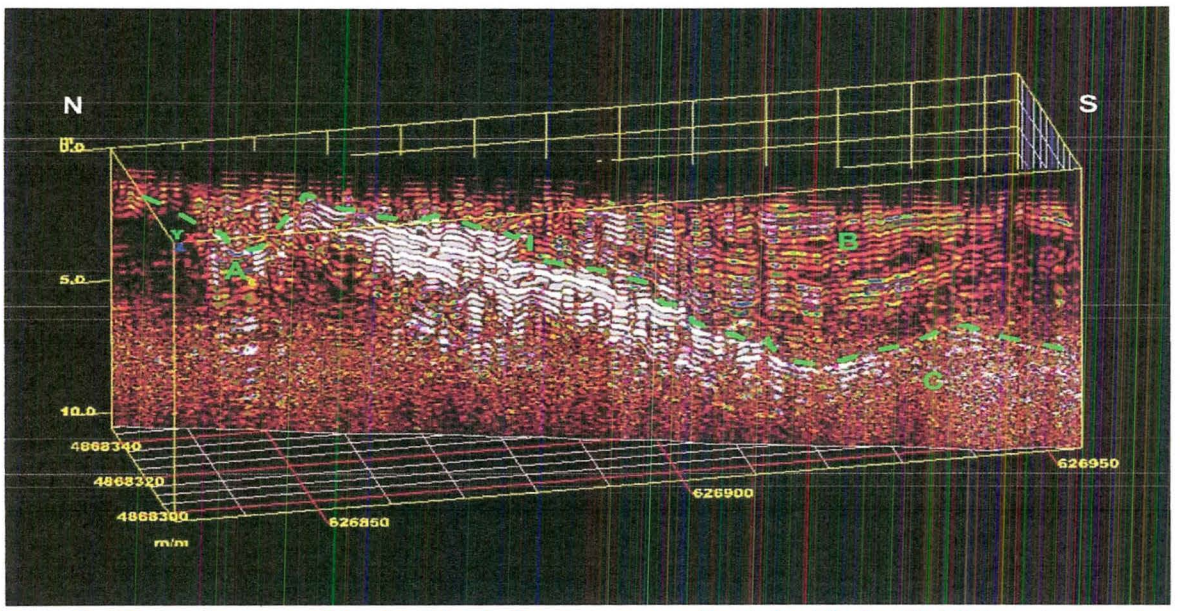

Figure 5. The radar record in this block diagram was collected with the 70 MHz antenna along traverse line T9. The subsurface depth and topography of the basaltic rock is highlighted with a green-colored segmented line.

In Figure 5, different layers of alluvial deposits are evident in the southern portion of the radar traverse (see "B"). These layers are relatively transparent to GPR and therefore assumed to consist of electrically resistive, low-clay content materials. No single stratigraphic layer stands out and can be continuously traced laterally (with confidence) across this section of the radar record. However, variations in the architecture of these strata can be discerned. Above "B" the strata appear horizontal. These geometries suggest level beds that differ in grain-size distribution, clay or organic matter contents. Skelly et al. (2003) and Bridge et al. (1998) associated parallel/planar reflectors with accretion or channel-filling during high-flow discharge events. Below "B" the strata appear more curved and concave upward. Skelly et al. (2003) and Bridge et al. (1998) associated similar reflection patterns with the infilling of an older erosional surface. In Figure 5, the curved and concave upward reflections below "B" mimic the topography of the basaltic rock surface. The aforementioned stratigraphic structure undoubtedly influences the flow of ground water.

Figure 6 is the radar record from traverse line T5 (see Figure 4 for location). This rather long traverse line crosses the east-central portion of the basin meadow. In Figure 6, the basaltic rock surface provides high-amplitude (colored white and gray) reflections that are easily traced across most of the radar record. However, in the northern portion of the radar record (in Figure 6, below "A"), this interface is lost due to its deeper depth and the cumulative effects of signal attenuation. In some areas (see "B"), reflections from the basaltic rock can be grouped into different layers each with different spatial reflection patterns. In Figure 6, on either side of "A", the alluvial strata appear to dip more precipitously downward suggesting infilling of a former erosional surface. The contrast in these alluvial layers is presumably

caused by differences in moisture contents associated with differences in grain-size distribution, density, clay content and/or organic matter content. These interfaces appear discontinuous. As noted by Skelly et al. (2003) and Bridge et al. (1998), reflections are more discontinuous on radar records that are collected across a channel, roughly perpendicular to the direction of flow. Reflections are more continuous on radar records that are collected along traverse lines orientated roughly parallel to the channel margins and the direction of flow.

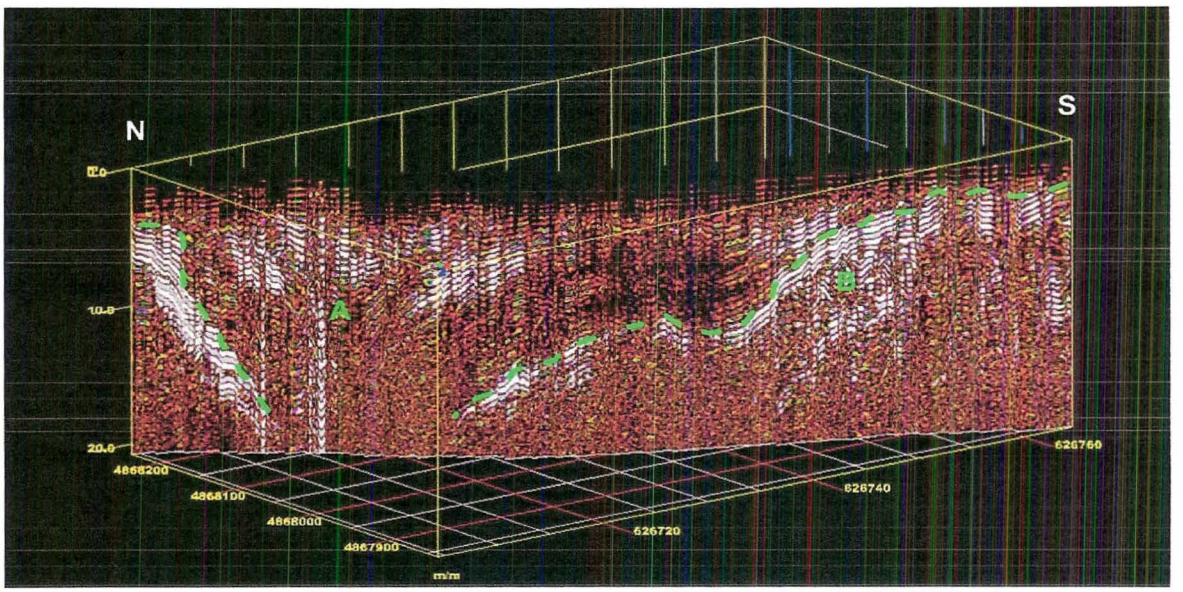

Figure 6. The radar record in this block diagram was collected with the 70 MHz along traverse line T5. The subsurface depth and topography of the basaltic rock has been highlighted with a green-colored segmented line.

Stratigraphic architecture:

The 200 MHz antenna was used to provide higher resolution of the stratigraphic architecture that overlie the basaltic rock. Figure 7 shows the approximate locations of twenty-four traverses that were completed with the 200 MHz antenna across the basin meadow

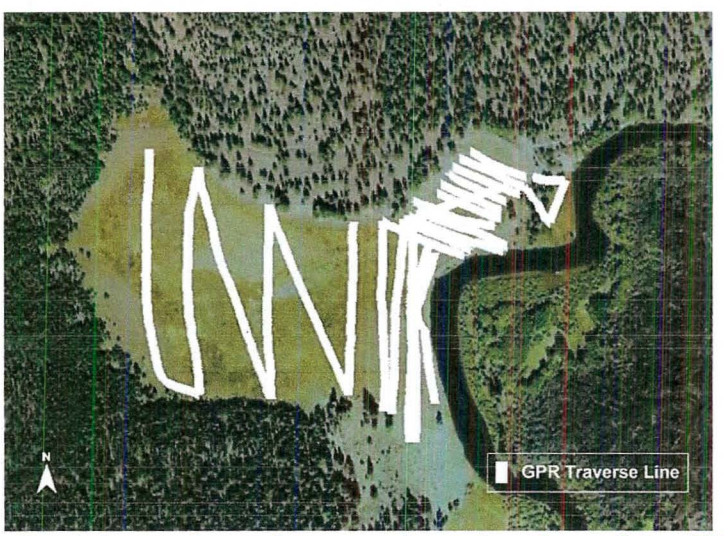

Figure 7. This Google Earth image shows the approximate locations of the GPR traverse lines that were completed with the 200 MHz antenna *(courtesy of Brian Jones of GSSI).*

Across the basin meadow, significant spatial variability in the stratigraphic architecture resulted in uncertainty concerning the identity and lateral continuity of interfaces on and among the radar records. Reflections varied in form, amplitude, and continuity. As a consequence, the identities of many closely spaced reflections were unclear and difficult to unravel. In the absence of adequate core data, only general inferences can be made concerning the identity and physical properties of the reflectors.

As discussed earlier, an attempt was made to identify and map the Mazama ash layer across the basin meadow. This major stratigraphic layer was known to vary in depth from 0.66 to 9.96 m (based on core data from 29 wells). Ground-penetrating radar traverses that were completed with the 200 MHz antenna passed in "the vicinity" of 19 of 29 well sites. On the resulting radar records, at each approximated well locations, a high amplitude subsurface reflection was initially identified as the likely Mazama ash layer. Like other strata appearing on radar records, the layer identified as the Mazama ash varied in amplitude, and was often discontinuous and variable in depth. These factors created interpretational uncertainties. Using a constant propagation velocity, the interpreted depth often varied considerably from the measured depth. As a result, the Mazama ash layer could not be consistently identified on radar records and was considered impractical to chart across the basin meadow.

Radar facies analysis was used to assess the stratigraphic architecture within the basin meadow. Facies analysis involves the recognition of visible differences in the expression and geometry of reflection patterns and the presence of bounding surfaces on radar records. Radar facies were defined by Baker (1991) as

> "Groups of radar reflections whose parameters (configuration, amplitude, continuity, frequency, interval velocity, attenuation, dispersion) differ from adjacent groups. Radar facies are distinguished by the types of reflection boundaries, configuration of the reflection pattern within the unit and the external form or shape of the unit."

Each radar facies is identified by its distinctive internal reflection patterns (based on reflection continuity, configuration, amplitude, dominant frequency, and degree of penetration). Bounding surfaces define and separate reflection patterns into distinct units or facies. Bounding surfaces generally represents erosional surfaces. Bounding surfaces are evident by the truncation of reflections and changes in reflection patterns on radar records. Anderson (1989) noted that a *radar facies* is considered a "homogenous, isotropic or anisotropic unit' that "is hydrogeologically relevant to groundwater flow and solute transport". However, as noted by Bayer et al. (2011) radar facies are not unique and must be defined for different depositional environments. In addition, Bristow (2009) noted that some different radar facies identified on 2D radar records may actually represent alternative views of the same 3D structure.

Figure 8 is a two-dimensional simulation of the Ryan Ranch Restoration Site showing the interpreted depth to basaltic rock using the variable velocity model. The locations and identities of 6 radar traverses that were completed with the 200 MHz antenna and will be discussed in this report are shown in this figure.

Figures 9 thru 14 are three-dimensional (3D) simulations of representative radar records collected with the 200 MHz antenna in different parts of the basin meadow. In each 3D simulation, measurements are expressed in meters. The UTM geographic coordinate system has been used to georeference the radar traverses in these simulations. In each 3D simulation, a green-colored, segmented line has been used to approximate the interpreted basaltic rock surface. The basaltic rock is labeled "A" in each of these simulations. In these simulations, the propagation velocity is constant (0.1547 m/ns) and the range is 108 ns. The use of these constants results in a maximum exploration depth for the 200 MHz antenna of 8.3 m. The resolution of the 200 MHz antenna (about 19 cm in these materials) does not permit all stratigraphic

layers to be depicted. In addition, because of the increasing size of the antenna's footprint, resolution decreases with increasing depth.

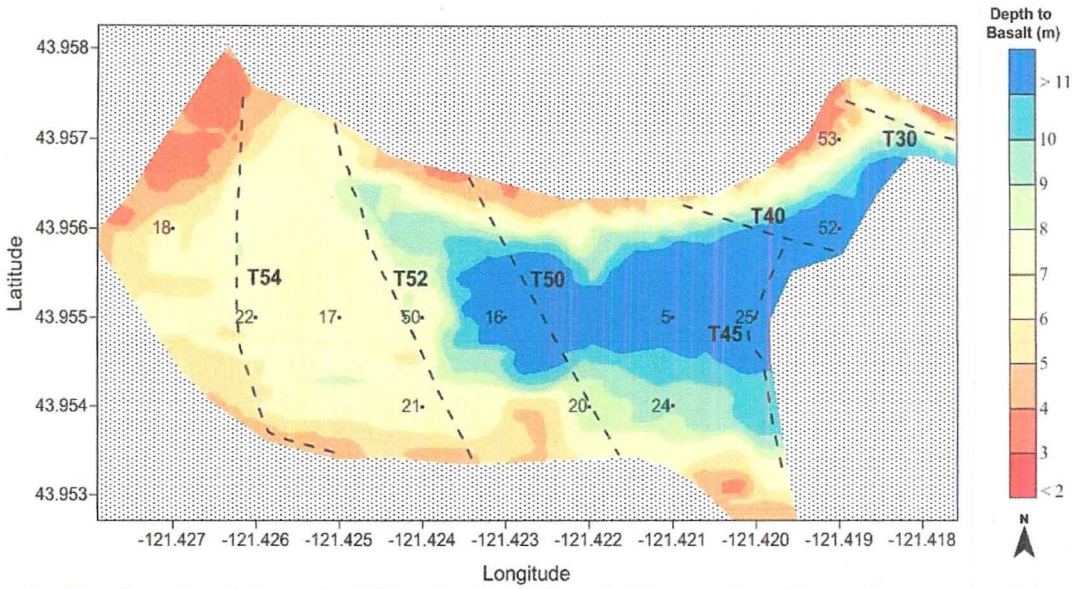

Figure 8. ***Depth to basaltic rock within the Ryan Ranch Restoration Site as interpreted from radar records using a variable velocity model. Bold numbers identify selected 200 MHz antenna traverse lines (dashed lines) and plain numbers identify well sites. All depths are expressed in meters.***

Figures 9 is the radar record from traverse line T40 (see Figure 8 for location). This traverse line is located in the western part of the basin meadow's eastern arm. This traverse crossed a drainage ditch, which caused an inflection and reduced signal amplitudes in the recorded data (see "F" in Figure 9).

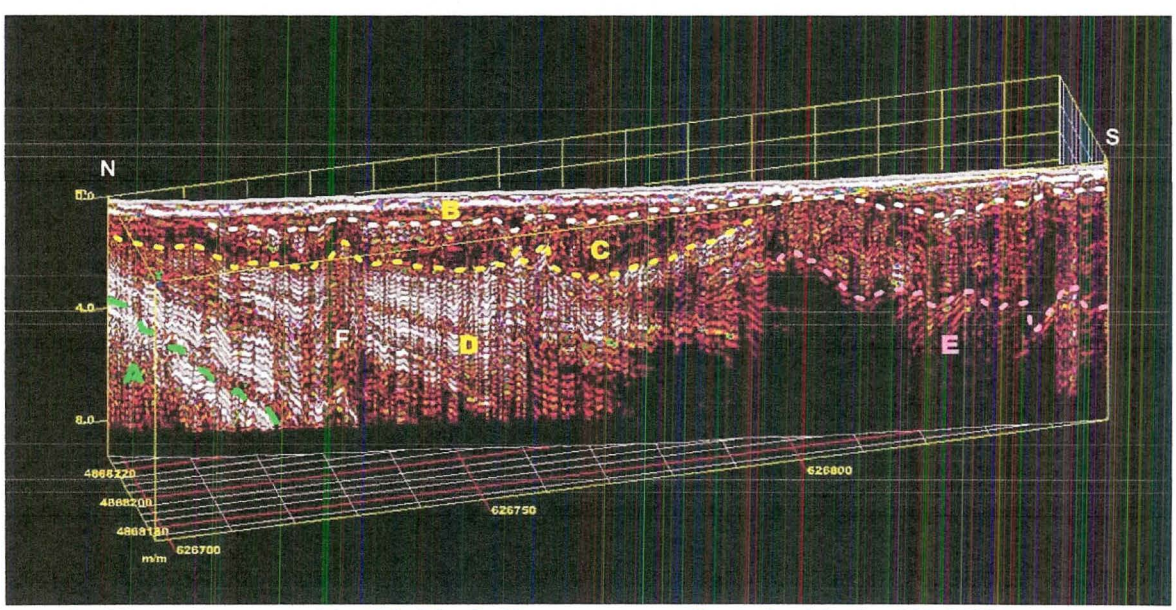

Figure 9. The radar record in this block diagram was collected with the 200 MHz antenna along traverse line T40. Various radar facies representing different stratigraphic units (B, C, D, and E have been identified. The subsurface depth and topography of the basaltic rock (A) has been highlighted with a green-colored segmented line.

In Figures 9, in the extreme, northern (left-hand) portion of T40, a plunging basaltic rock surface has been highlighted. For the remainder of this traverse, the depth to basaltic rock is beyond the maximum depth of exploration (about 8 m). The upper part of the basaltic rock ("A") consists of multiple high-amplitude (colored white and gray) reflectors. The high amplitude signifies highly contrasting layers and inhomogeneities within the upper part of the basaltic rock.

On the radar record shown in Figure 9, a white-colored, segmented line has been used to identify a continuous, nearly level, bounding surface in the upper part of the radar record. The estimated depth to this bounding layer ranges from about 60 to 160 cm. This reflector varies laterally in amplitude, is highly segmented, and difficult to trace across the radar record. Above and below this surface are two distinctly different radar patterns or *radar facies* ("B" and "C"). Above this bounding surface, radar facies "B" is characterized by low- to moderate-amplitude, discontinuous, wavy, sigmoidal (curved at both ends) and planar reflectors, and point reflectors. The sigmoidal and planar reflectors are nearly level to slightly inclined and represent near surface soil horizons and stratigraphic layers. The point reflectors may represent soil inhomogeneities, larger rock fragments, or animal burrows. Radar facies "C" is characterized by highly segmented, low-to high amplitude, chaotically arranged point, sigmoidal and planar reflectors with extensive areas having little or no signal returns (colored black). In other studies, chaotic reflection patterns have been associated with colluvium and till.

In Figure 9, a yellow-colored, segmented line has been used to identify a bounding surface separating facies "C" from the underlying facies "D". Facies "D" consists of multiple, moderate- to high-amplitude, more continuous, inclined, planar reflectors. Similar high-angled, inclined reflections have been associated with glaciofluvial, alluvial, and aeolian sediments (van Overmeeren, 1998).

In the southern (right-hand) portion of traverse T40, a pink-colored, segmented line has been used to identify a bounding surface that separates facies "C" from facies "E". Facies "E" consists of low amplitude, inclined planar reflectors that are rapidly attenuated with increasing depth. Excessive attenuation restricts the depth of signal penetration in facies "E". Though not verified, the higher rates of signal attenuation may be associated with higher clay and moisture contents. It is unclear whether facies "E" is unique or represents a continuation of facies "D".

Figures 10 is the radar record from traverse line T30 (see Figure 8 for location). Compared with other traverses completed in the eastern arm of the basin meadow, the depth to basaltic rock ("A") is relatively shallow along this traverse line. The surface of the basaltic rock is irregular over short distances and plunges below the maximum exploration depth (about 8 meters) in the central portion of this traverse. Once again, the upper part of the basaltic rock consists of multiple high-amplitude (colored white and gray) reflectors that signify highly contrasting layers and inhomogeneities.

On the radar record shown in Figure 10, a white-colored, segmented line has been used to identify a continuous, nearly level, bounding surface. The estimated depth to this surface ranges from about 90 to 185 cm. This traverse passed close to well # 9, where the depth to Mazama ash occurs at a depth of 177 cm. Accordingly, this bounding surface and interface may represent the upper surface of the Mazama ash layer. Reflections from this bounding surface are variable in amplitude (from low (colored black and red) to high (colored white and gray)), appear highly segmented, and are difficult to trace laterally across the radar record. These characteristics suggest possible reworking and variations in the physical properties (changes in grain-size distributions, porosity, and clay, organic matter, and/or moisture contents) of this stratum and the overlying materials. As in radar traverse T40, above this bounding surface is facies "B". In general, on this simulation, facies "B" largely consists of relatively low-amplitude, discontinuous, nearly-level, sigmoidal and planar reflections, with areas of no signal return and an occasional point reflector. The relatively low amplitudes of these reflectors suggest a lack of grain-size/compositional contrasts in the sediments that make up facies "B".

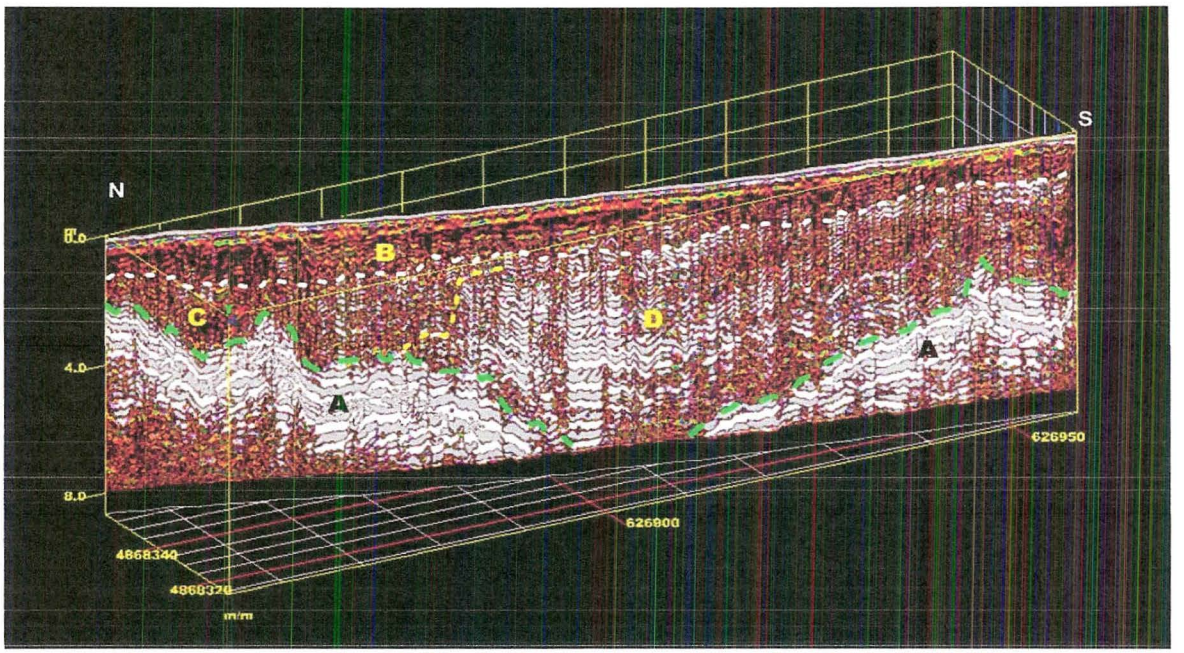

Figure 10. The radar record in this block diagram was collected with the 200 MHz antenna along traverse line T30. Various radar facies representing different stratigraphic units (B, C, and D) have been identified. The subsurface depth and topography of the basaltic rock (A) has been highlighted with a green-colored segmented line.

In Figure 10, in the extreme northern (left-hand) portion of traverse line T30, below the nearly level bounding surface (white-colored, segmented line), a unit of chaotically arranged sigmoidal and planar reflectors, having limited areas of no signal return, is evident. This reflection pattern is associated with facies "C". In this portion of the radar record, a yellow-colored, segmented line has been used to represent the bounding surface that separates facies "C" from facies "D". This bounding surface and facies "C" are not present in the central and southern portions of this traverse. Here, facies "B" appears to be underlain directly by facies "D". Facies "D" is composed of multiple, moderate- to high-amplitude, planar and sigmoidal reflections. These reflections are inclined and slope downwards toward the mid-section of the traverse where the underlying basaltic rock surface is the deepest. The overall 2D pattern within facies "D" is concave-upwards. This reflection pattern is interpreted as fill deposits on an older surface, possibly a former stream or river channel. The reflectors in facies "D" are discontinuous, which is characteristic of deposits profiled in a cross-channel direction with GPR.

Figures 11 is the radar record from traverse line T45 (see Figure 8 for location). This traverse line extends across both the eastern and southern arms of the basin meadow and closely follows and is located near the levee to the Upper Deschutes River. The underlying basaltic rock ("A") is only evident in the extreme southern (right-hand) portion of this 3D simulation. In other portions of this traverse, the depth to basaltic rock exceeds the maximum exploration depth.

Along this traverse, a new sub-facies, facies "B1" is introduced. Facies "B1" is similar to facies "B" as it is near-surface and largely consists of relatively low-amplitude, discontinuous, nearly-level, sigmoidal and planar reflections. However, compared to facies "B", facies "B1" is thicker, extends to deeper depths, and has more noticeable areas of no signal return.

A white-colored, segmented line has been used to approximate the nearly level to undulating, bounding surface that separates facies "B1" from "D". Estimated depths to this bounding surface range from about

1.4 to 3.6 m. In the southern portion (right-hand portion of Figure 11) of this traverse, this bounding surface is deeper, better defined, and more easily charted. In the northern part (left-hand portion of Figure 11) of this traverse, this bounding surface is shallower, more segmented, and difficult to identify. Near the abrupt change in direction on this 3D simulation, traverse T45 passed near well #51, where the depth to Mazama ash is 4.26 m. In the vicinity of this well, the interpreted depth to this bounding surface (segmented white-colored line) on this radar record was only 1.47 m. Additional borings will be required to confirm the identity of this interface and the short-range variability in the depth to Mazama ash.

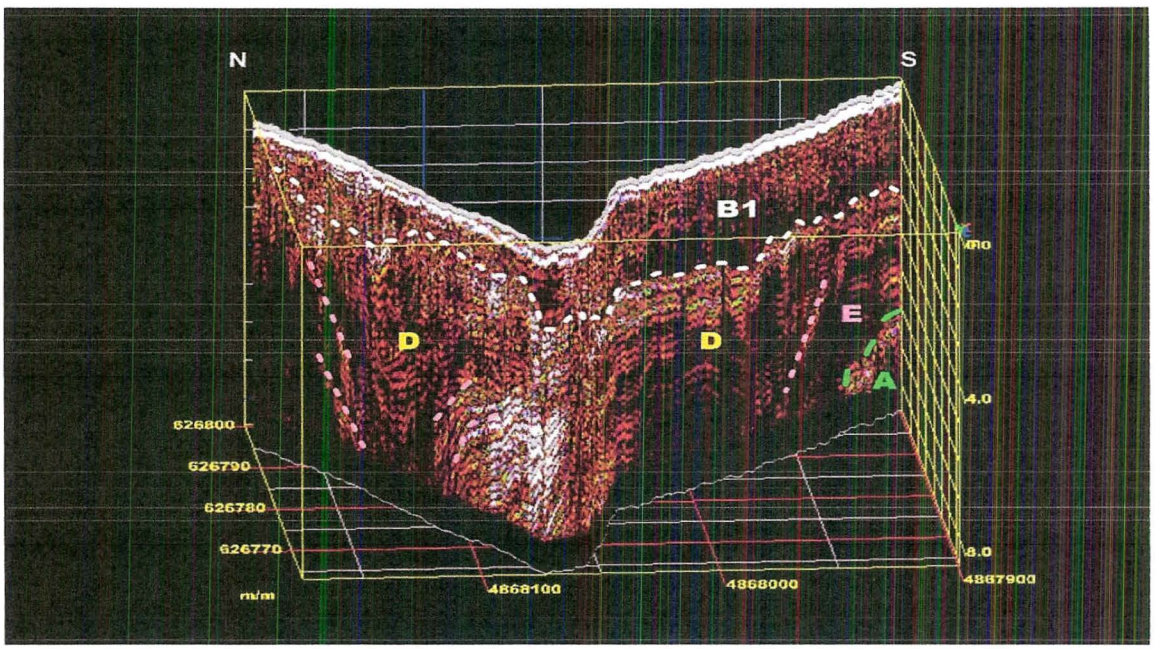

Figure 11. The radar record in this block diagram was collected with the 200 MHz antenna along traverse line T45. Various radar facies representing different stratigraphic units (B1, D, and E) have been identified. The subsurface depth and topography of the basaltic rock (A) has been highlighted with a green-colored segmented line.

Facies "C", which consists of mostly low amplitude, chaotically arranges sigmoidal and planar reflectors, was not identified along traverse T45.

In Figure 11, Facies "D" consists of inclined and curved upwards, sigmoidal and planar reflectors. In fluvial settings, similar reflectors have been associated with lateral and oblique flow and alluvial deposition into former troughs (Skelly et al., 2003; and Bridge et al., 1998). Near the abrupt curvature in this 3D simulation, these layered reflectors become more intense in amplitude (implying more physically contrasting materials). These reflectors continue into the southern portion of the radar traverse where they appear lower in amplitude (less physically contrasting) and more horizontal. The lower amplitude of these reflections may be the result of saturated conditions as this portion of the traverse closely follows the edge of the levee and the Upper Deschutes River. Increased moisture contents weaken the propagated radar signal and can dilute or mask some subsurface interfaces. In the northern portion of this traverse, reflectors are more steeply inclined, concave-upwards in cross-section, and more similar to the previously discussed reflectors of facies "D" in the eastern arm of the basin meadow (traverse lines T30 and T40).

In the extreme southern portion of T45, a pink-colored, segmented line has been drawn to identify a bounding layer believed to separate facies "D" from facies "E". Facies "E" consists of low amplitude, inclined planar reflectors that are rapidly attenuated with increasing depth. Excessive attenuation restricts

the depth of signal penetration in facies "E". It is unclear whether facies "E" should be identified as separate facies or an alternative expression of facies "D".

Figures 12 is the radar record from traverse line T50 (see Figure 8 for location). This traverse line extends across the western arms of the basin meadow. On either ends of this traverse line, moderate- to high-amplitude, oblique planar and sigmoidal reflectors represent the plunging basaltic rock surface. For the majority of this traverse line, the surface of the basaltic rock is deeper than the depth of exploration (about 8 m).

Along traverse line T50, below the surface layers, near surface materials (facies "B1") are characterized by low- to moderate-amplitude, discontinuous planar and sigmoidal reflectors. The absence of high-amplitude reflections in these near surface materials suggests physically similar materials. These reflectors are nearly level to slightly undulating and associated with alluvial fill deposits. Compared with facies "B" on the radar records obtained in the eastern arm of the basin meadow, along traverse T50, facies "B1" contains lengthier linear reflections and more noticeable areas of no signal return. The western arm of the basin meadow is more distant from the Upper Deschutes River, but is wetter. These differences may explain the perceived difference in facies "B" and "B1" between the two arms of the basin.

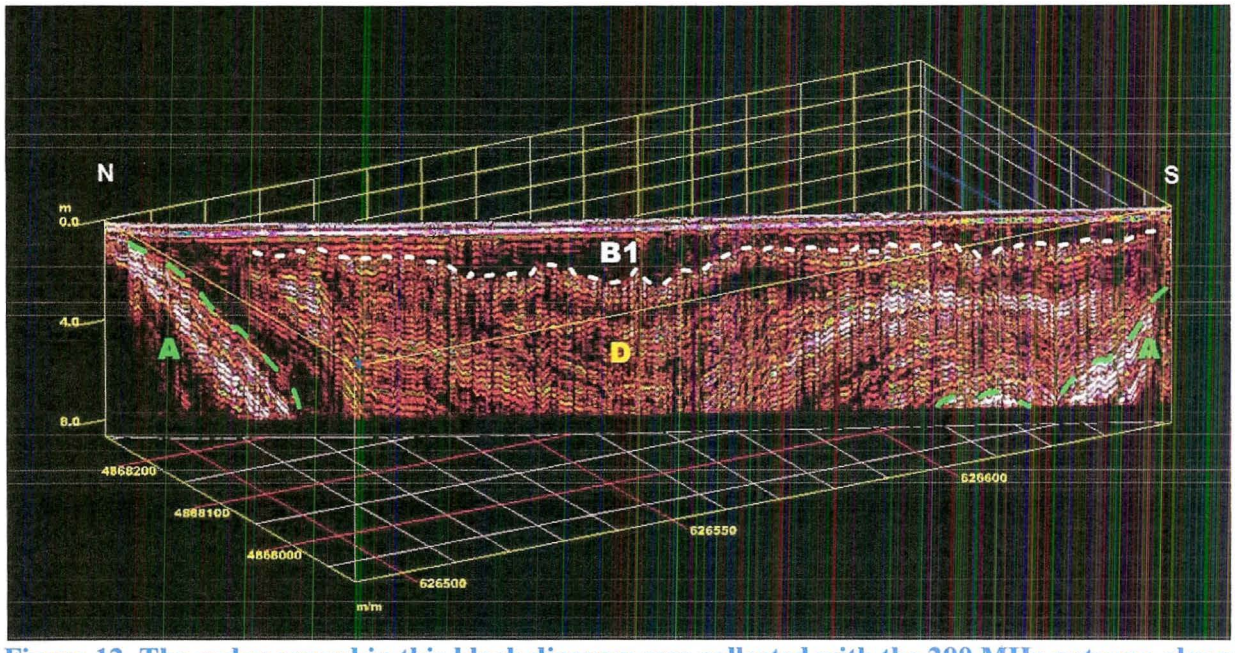

Figure 12. The radar record in this block diagram was collected with the 200 MHz antenna along traverse line T50. Two radar facies representing different stratigraphic units (B1 and D) have been identified. Where within the depth of exploration, the subsurface depth and topography of the basaltic rock (A) has been highlighted with a green-colored segmented line.

On the radar record shown in Figure 12, a white-colored, segmented line has been used to highlight the bounding surface that separates facies "B1" from facies "D". Along this traverse, the estimated depth to this bounding surface ranges from about 0.9 to 3.1 m. This traverse did not passed near any wells, but the depth, general expression, and continuity of this layer suggests that it possibly represent the Mazama ash layer. Underlying this bounding layer is radar facies "D". Facies "D" consists of multiple, discontinuous, undulating, inclined reflectors that appear to fill a large trough or depression, which is presumed to represent and older channel or erosional surface. A majority of these reflectors are concave-upwards in cross section. These reflectors have noticeably lower amplitudes than similar reflectors from this facies

that are evident in the radar records (T30 and T40) from the eastern arm of the basin meadow. In Figure 12, in the upper part of facies "D", immediately below the bounding surface, large areas of no signal return are evident. Perhaps this general area should have been included in another facies. No facies "C", which is characterized by chaotically arranged sigmoidal and planar reflectors, is evident along this traverse.

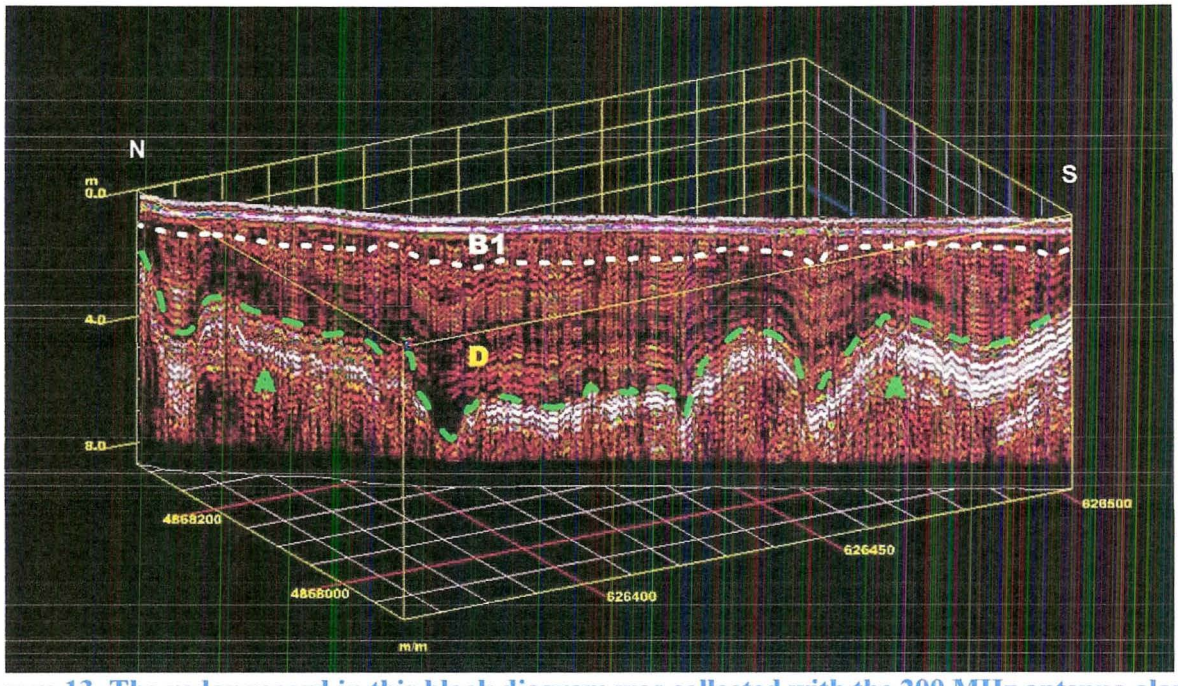

Figure 13. The radar record in this block diagram was collected with the 200 MHz antenna along traverse line T52. Two radar facies representing different stratigraphic units (B1 and D) have been identified. The subsurface depth and topography of the basaltic rock (A) has been highlighted with a green-colored segmented line.

Figures 13 is the radar record from traverse line T52 (see Figure 8 for location). This traverse line also extends across the western arms of the basin meadow and is located a short distance to the west of traverse line T50. Soils are principally poorly drained and very poorly drained with areas of relatively thick organic layers along traverse T52. Along traverse line T52, the underlying basaltic rock is noticeably shallower than in previous traverses and can be traced laterally across the entire radar record at depths ranging from about 1.6 to 7.2 m. In this simulation, the topography of the basaltic rock is highly irregular with four noticeable deep cavities and several shallower, more undulating surfaces.

In Figure 13, facies "B1" is composed of low- to moderate-amplitude, segmented linear and sigmoidal reflections. The numbers of reflections in facies "B1" appear to diminish from east to west (traverse lines T45, T50 and T52) across the western arm of the basin meadow. This may be due to the increased wetness and the presence of a thicker organic mat. Similar to facies "B1" in traverse T50, reflectors are nearly level to slightly undulating. No facies "C", which is characterized by chaotically arranged sigmoidal and planar reflectors, with noticeable areas with no signal return, is evident in this and all traverses conducted in the western arm of the basin meadow.

On the radar record shown in Figure 13, a white-colored, segmented line has been used to highlight the bounding surface that separates facies "B1" from facies "D". Facies "D" consists of low- to moderate amplitude, wavy to hummocky sigmoidal reflectors that appear to conform to the general topography of the underlying basaltic rock surface. Compared with the reflectors from this facies in the eastern arm of

the basin meadow, these layered reflectors appear lower in signal amplitude, more horizontal and less inclined, with more noticeable areas of no signal return. In the basin meadow's eastern arm, facies "D" is composed of higher-amplitude reflections. The lower amplitude of reflections from facies "D" in the western arm suggests the presence of less contrasting materials and possibly the diluting affects of increased moisture contents.

Figures 14 is the radar record from traverse line T54 (see Figure 8 for location). This traverse is the western-most line completed with the 200 MHz antenna across the western arms of the basin meadow. Similar to traverse line T52, along traverse T54, soils are generally poorly drained and very poorly drained with relatively thick organic layers. However, in contrast to the radar record from traverse T52, along T54, the basaltic rock surface is more discontinuous, weakly expressed, and difficult to identify. These characteristics of the basaltic rock surface may reflect wetter conditions resulting in increased signal attenuation.

Along traverse line T54, the underlying basaltic rock is relatively shallow and has been traced laterally across the radar record at depths ranging from about 1.3 to 5.4 m. In portions of this traverse, the surface of the basaltic rock has been traced along moderate-amplitude reflections. Immediately below these reflections are zones of little or no signal return that signifies fairly homogenous materials. In these segments of T52, the contrast between the basaltic rock and the overlying sediments is also less pronounced, which suggests more intense weathering or a more pitted or irregular basaltic rock surface. In addition the basaltic rock surface is more segmented and difficult to follow. These characteristics may reflect a more irregular surface and/or the effects of signal attenuation. The shallow depth to basaltic rock in these sections needs to be verifies.

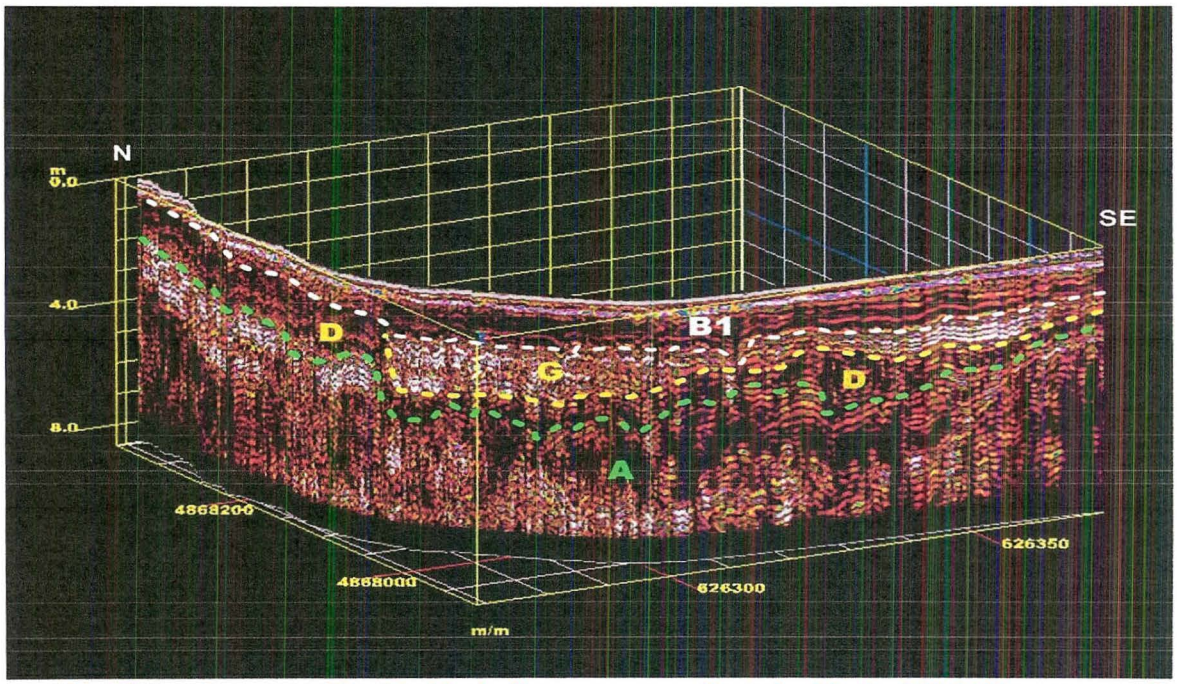

Figure 14. The radar record in this block diagram was collected with the 200 MHz antenna along traverse line T54. Various radar facies representing different stratigraphic units (B1, D, and G) have been identified. The subsurface depth and topography of the basaltic rock (A) has been highlighted with a green-colored segmented line.

On the 3D simulation shown in Figure 14, a white-colored, segmented line has been used to identify the top of a prominent, continuous, nearly level, bounding surface. Along this traverse, the estimated depth

to the bounding layer ranges from about 1.4 to 2.6 m. In Figure 14, facies "B1" is composed of low- to moderate-amplitude, segmented linear and sigmoidal reflections. Similar to facies "B1" in traverses T50 and T52, these reflectors are nearly level to slightly undulating. Noticeable areas of no signal return in facies "B1" suggest areas of relatively homogenous materials. In the northern (left-hand) portion of this simulation, facies "D" has been identified. This facies is associated with wavy to inclined, segmented, lower- amplitude reflections that are often concave-upwards in cross section with significant areas of no signal return. Unlike facies "D" in the previously discussed traverses, in traverse T54, this facies is thin, weakly expressed, and perhaps more elusive to define and visualize. In the southern portion of traverse T54, a new facies, facies "G" has been identified. This facies consists of nearly level, high- and moderate-amplitude, sub-parallel, planar and sigmoidal reflectors that generally conform with many of the characteristics of facies "D", other than being seemingly more attenuating. Beneath facies "G", the basaltic rock is more poorly expressed. The lower amplitude of the basaltic rock beneath facies "G" may be the result of the overlying materials, especially those comprising facies "G" having higher clay and moisture contents and being more attenuating to the radar signal.

References:

Anderson, M.P., 1989. Hydrogeologic facies models to delineate large-scale spatial trends in glacial and glaciofluvial sediments. *Geological Society of America Bulletin* 101: 501-511.

Baker, P.L., 1991. Response of ground penetrating radar to bounding surfaces and lithofacies variations in sand barrier sequences. *Exploration Geophysics* 22: 19-22

Bayer, P., P. Huggenberger, R. Renard, and A. Comunian, 2011. Three-dimensional high resolution fluvial-glacial aquifer analog: part 1: Field study. *Journal of Hydrology* 405: 1-9.

Beres, M. and F. P. Haeni, 1991. Application of ground-penetrating-radar methods in hydrogeologic studies. *Ground Water* 29(3): 375-386.

Bridge, J., R. Collier, and I. Alexander, 1998. Large-scale structure of Calamus River deposits (Nebraska, USA) revealed using ground-penetrating radar. *Sedimentology* 45: 977-986.

Bridge, J.S., N.D. Smith, F. Trent, S.L. Gabel, and P. Bernstein, 1986. Sedimentology and morphology of a low-sinuosity river: Calamus River, Nebraska Sandhills. *Sedimentology* 33: 851-870.

Bristow, J., 2009. Advances in fluvial sedimentology using GPR. In *Ground Penetrating Radar: Theory and Applications*, ed. H. M. Jol, 323-359 pp. Elsevier Science, Amsterdam, The Netherlands.

Cassidy, N.J. 2009. Electrical and magnetic properties of rocks, soils, and fluids. In *Ground Penetrating Radar: Theory and Applications*, ed. H. M. Jol, 41-72 pp. Elsevier Science, Amsterdam, The Netherlands.

Collins, M. E., J. A. Doolittle, R. V. Rourke, 1989. Mapping depth to bedrock on a glaciated landscape with ground-penetrating radar. *Soil Science Society of America Journal* 53(3): 1806-1812.

Conyers, L.B. and D. Goodman, 1997. Ground-Penetrating Radar: An introduction for Archaeologists. AltaMira Press, Walnut Creek, California.

Dagallier, G., A. I. Laitinen, F. Malartre, I. P. Van Campenhout, and P. C. H. Veeken, 2000. Ground penetrating radar application in a shallow marine Oxfordian limestone sequence located on the eastern flank of the Paris Basin, NE France. *Sedimentary Geology* 130: 149-165.

Daniels, D.J., 2004. *Ground Penetrating Radar; 2nd Edition*. The Institute of Electrical Engineers, London, United Kingdom.

Davis, J.L., and A.P. Annan. 1989. Ground-penetrating radar for high-resolution mapping of soil and rock stratigraphy. *Geophysical Prospecting*, 37: 531-551.

Demanet, D., L. G. Evers, H. Teerlynck, B. Dost, and D. Jongmans, 2001. Geophysical investigations across the Peel boundary fault (The Netherlands) for a paleoseismological study. *Netherlands Journal of Geosciences* 80 (3-4): 119-127.

Gómez-Ortiz, D., T. Martín-Crespo, S. Martín-Velázquez, and P. Martínez-Pagán, 2010. Application of ground penetrating radar (GPR) to delineate clay layers in wetlands. A case study in the Soto Grande and Soto Chico watercourses, Doñana (SW Spain). *Journal of Applied Geophysics* 72: 107-113.

Gerber, R., P. Felix-Henningsen, T. Behrens, and T. Scholten, 2010. Applicability of ground-penetrating radar as a tool for nondestructive soil-depth mapping of Pleistocene periglacial slope deposits. *Journal of Plant Nutrition and Soil Science* 173: 173-184.

Jol, H., 2009. *Ground Penetrating Radar: Theory and Applications*. Elsevier Science, Amsterdam, The Netherlands.

Lane, J. W., M. L. Buursink, F. P. Haeni, and R. J. Versteeg, 2000. Evaluation of ground-penetrating radar to detect free-phase hydrocarbons in fractured rocks – results of numerical modeling and physical experiments. *Ground Water* 38(6): 929-938.

Leclerc, R.F., and E.J. Hickin, 1997. The internal structure of scrolled floodplain deposits based on ground-penetrating radar, North Thompson River, British Columbia. *Geomorphology* 21: 17-38.

Mysaiah, D., K. Maheswari, M. Srihari Rao, P. Senthil Kumar, and T. Seshunarayana, 2011. Ground-penetrating radar applied to imaging sheet joints in granite bedrock. *Current Science* 100(4): 473-475.

Nascimento da Silva, C. C., W. E. de Medeiros, E. F. Jarmin de Sa, and P. X. Neto, 2004. Resistivity and ground-penetrating radar images of fractures in a crystalline aquifer: a case study in Caicara farm – NE Brazil. *Journal of Applied Geophysics* 56: 295-307.

Neil, A., 2004. Ground-penetrating radar and its uses in sedimentology: principles, problems and progress. *Earth Science Reviews* 66: 261-330.

O'Driscoll, M., P. Johnson, and D. Mallinson, 2010. Geologic controls and effects of floodplain asymmetry on river-groundwater interactions in the southeastern Coastal Plain, USA. *Hydrogeology Journal* 18: 1265-1279.

Pipan, M., L. Baradello, E. Forte, and A. Prizzon, 2000. GPR study of bedding planes, fractures and cavities in limestone. 682-687. *In*: Noon, D. (ed.) Proceedings Eight International Conference on Ground-Penetrating Radar. May 23 to 26, 2000, Goldcoast, Queensland, Australia. The University of Queensland.

Porsani, J. L., V. R. Elis, and F. Y. Hiodo, 2005. Geophysical investigations for the characterization of fractured rock aquifer in Itu, SE Brazil. *Journal of Applied Geophysics* 57: 119-128.

Rubin, Z., S.L. Rathburn, E. Wohl, and D.L. Harry, 2012. Historic range of variability in geomorphic processes as a context for restoration: Rocky Mountain National Park, Colorado, USA. *Earth Surface Processes and Landforms* 37: 209-222.

Sambrook Smith, G.H., P.J. Ashworth, J.L. Best, J. Woodward, and C.J. Simpson, 2006. The sedimentology and alluvial architecture of the sandy braided South Saskatchewan River, Canada. *Sedimentology* 56: 413-434.

Sass, O., 2007. Bedrock detection and talus thickness assessment in the European Alps using geophysical methods. *Journal of Applied Geophysics* 62: 254-269.

Skelly, R.L., C.S. Bristow, and F.G. Ethridge, 2003. Architecture of channel-belt deposit in an aggrading shallow sandbed braided river: the lower Niobrara River northeast Nebraska. *Sedimentary Geology* 158: 249-270.

Theune, U., D. Rokosh, M. D. Sacchi, and D. R. Schmitt, 2006. Mapping fractures with GPR: A case study from Turtle Mountain. *Geophysics* 71(5): B139-B150.

Vandenberghe, J. and R.A. van Overmeeren, 1999. Ground penetrating radar images of selected fluvial deposits in the Netherlands. Sedimentary Geology 128: 245-270.

van Overmeeren, R.A., 1998. Radar facies of unconsolidated sediments in The *Netherlands: A radar stratigraphy interpretation method for hydrogeology. Journal* of Applied Geophysics 40: 1-18.